

Oblique Wave Interaction With Flexible Plate in Ocean of Uneven Bottom

Saista Tabssum¹ and Balaji Ramakrishnan²

Received: 15 March 2023 / Accepted: 25 June 2023

© Harbin Engineering University and Springer-Verlag GmbH Germany, part of Springer Nature 2024

Abstract

The present work analyzes the interaction of oblique waves by a porous flexible breakwater in the presence of a step-type bottom. The physical models for both scattering and trapping cases are considered and developed within the framework of small amplitude water-wave theory. Darcy's law is used to model the wave interaction with the porous medium. It is assumed that the varying bottom extends over a finite interval, connected by a finite length of uniform bottom near an impermeable wall, and a semi-infinite length of bottom in the open water region. The boundary value problem is solved using the eigenfunction expansion method in the uniform bottom regions, while a modified mild-slope equation (MMSE) is used for the region with the varying bottom. Additionally, a mass-conserving jump condition is employed to handle the solution at slope discontinuities in the bottom. A system of equations is derived by matching the solutions at interfaces. The reflection coefficient and force on the breakwater and impermeable wall are plotted and analyzed for various parameters, such as the length of the varying bottom, depth ratio, angle of incidence, and flexural rigidity. It is observed that moderate values of flexural rigidity and depth ratio significantly contribute to an optimum reflection coefficient and reduce the wave force on the wall and breakwater. Remarkably, the outcomes of this study are assumed to be applicable in the construction of this type of breakwater in coastal regions.

Keywords Porous flexible breakwater; Varying bottom; Mild-slope equation; Reflection coefficient; Wave force

1 Introduction

In recent decades, the mathematical study of the performance of breakwaters has received significant attention in order to protect coastal regions and attenuate wave energy. There has been a rise in interest in the use of flexible break-

waters as an alternative to the more conventional rigid type breakwaters in coastal regions, particularly where a poor sea bed exists. However, it is necessary for the transmitted and reflected wave heights to be small, which is why porous structures can be used effectively to dissipate wave energy. Moreover, flexible breakwaters are reusable and cost-effective for protecting marine structures from destructive waves. Additionally, these types of breakwaters generate fewer hydrodynamic forces. Therefore, the study of the performance of flexible porous breakwaters in predicting wave motion is of great importance in coastal engineering practice.

Meanwhile, fair developments have been made in both the theoretical and experimental investigation of the porous breakwater, with and without flexibility. Several mathematical tools have been formulated to deal with various shapes of porous barriers. A porous wave maker theory was developed by Chwang (1983) to study the small amplitudes of water waves raised by horizontal oscillations of a permeable barrier in uniform bottom. The hydrodynamic performance of submerged and surface-piercing permeable barriers in deep water was studied by Sahoo (1998) using logarithmic singular integral equations. Furthermore, Lee and Chwang (2000) used the least square method to analyze the effect of partial porous breakwaters of various configurations on the scattering of water waves. This analysis was extended by Sahoo et al. (2000), who studied the trapping and generation of normally incident water waves by con-

Article Highlights

- The article investigates the interaction of oblique waves by a porous flexible breakwater in the presence of a step-type bottom.
- The problem is analyzed under the framework of small amplitude water wave theory.
- The physical problem is solved using the eigenfunction expansion method in the uniform bottom regions, while a MMSE is used for the region of varying bottom.
- It is noticed that moderate values of flexural rigidity and depth ratio contribute significantly to obtain optimum reflection coefficient and reduce the wave force on the wall and breakwater.
- Effect of Bragg resonance is studied. A smaller depth ratio allows for higher reflection and least transmission in the case of wave scattering.

✉ Saista Tabssum
zebaxavier@gmail.com

¹ School of Advanced Science-Mathematics, VIT-AP, Amravati, 744101, India

² Department of Civil Engineering, Indian Institute of Technology, Bombay 400076, India

sidering an impermeable back wall. The trapping of water waves by two different kinds of porous flexible breakwaters, namely bottom standing and surface piercing, was studied by Yip et al. (2002). Williams and Wang (2003) investigated the hydrodynamics of flexible breakwaters to enhance the effectiveness of wetlands habitat restoration projects. Li et al. (2006) investigated the values of the porous effect parameter of thin porous breakwaters theoretically and experimentally. The problem of water wave scattering by a porous breakwater was converted to a second-kind hypersingular integral equation by Gayen and Mondal (2014) and analyzed for finite and infinite depth water. Using Babinet's principle, Manam and Sivanesan (2016) analyzed wave scattering by a porous barrier in deep water by demonstrating a connection between two wave potentials. Furthermore, a detailed study on oblique wave scattering and trapping was carried out by Koley et al. (2015) and Kaligatla et al. (2015) by converting the boundary value problem into a system of three Fredholm-type integral equations using Green's function. Das and Bora (2018) analyzed the performance of reflection and transmission coefficients for two vertical unequal porous breakwaters. Krishna et al. (2023) studied the interaction of oblique waves with porous block in the presence of thin permeable breakwater. Recently, Krishendu and Balaji (2020) conducted a numerical and experimental investigation on wave trapping by a porous breakwater placed in front of an impermeable rigid wall. Gupta et al. (2022) analyzed the scattering of water waves by two vertical porous flexible plates using Havelock's theorems for water waves.

In the previously mentioned articles, hydrodynamics of water waves were analyzed in uniform water depth however significant changes in wave characteristics occur due to bottom variation. Hence, there is a need to understand the refraction diffraction effects caused by the varying bottom. The refraction diffraction effect induced by varying bottom is examined with the help of the mild-slope equation which was derived by Berkhoff (1973) by using vertical averaging technique. Next, Chamberlain and Porter (1995) derived a modified mild-slope equation by employing the variational principle. The study of water wave interaction with a breakwater in the presence of varying bottoms is often important to understand the characteristics of waves to address more realistic physical problems. Suh and Park (1995) studied the reflection and transmission coefficients by porous breakwater in the presence of step-type bottom. However, they did not ensure the conservation of mass at the bottom slope discontinuity. The mass conserving jump condition is deduced by Porter and Staziker (1995) by addressing the effect of evanescent mode in the study of Chamberlain and Porter (1995). The application of modified mild-slope equation along with jump condition can be seen in the article of Behra et al. (2015) who studied oblique wave trapping by porous breakwater in the presence of step-type bottom.

Further, their model was extended by Kaligatla et al. (2018) who investigated the oblique wave scattering by multiple porous breakwaters in the water of varying depth. Recently, Venkateswarlu and Karmakar (2020) examined the significance of variable step-type bottom characteristics on wave trapping by stratified porous breakwaters.

The objective of the present article is to investigate the wave trapping and scattering by flexible porous breakwater by taking into account the effect of the varying bottom. The porous breakwater is assumed to be fixed at the bottom and placed in front of impermeable wall. The problem is examined under the framework of small amplitude water wave theory and Darcy's law is used to study flow past porous medium. The present physical problem is modeled by employing the MMSE of Chamberlain and Porter (1995) for the region of the varying bottom along with eigenfunction expansion method for flat bottom. The obtained solution in each region is matched at interface along with mass conserving jump condition at slope discontinuity. The system of algebraic equations is obtained and solved numerically to determine the unknown coefficients. Various physical quantities such as reflection coefficient, and wave force exerting on breakwater and wall are plotted and analyzed for several parameters. Moreover, several outcomes associated with the present problem are analyzed, validated, and compared with the known results available in the literature.

2 Statement of the boundary value problems

In the present work, the interaction between oblique waves and thin flexible breakwater is studied in the presence of varying bottom. Oblique wave trapping and scattering by thin porous flexible breakwater is formulated through Cartesian coordinate system (x, y, z) . The present Boundary Value Problem is modeled in the framework of small amplitude water-wave theory. The free surface is assumed to be undisturbed and lying on the xy -plane and z -axis being in a positive upward direction. The bottom of sea is assumed to be impermeable and varying bottom at $z = -h_2(x)$ is spanned over $0 \leq x \leq L$ is connected by two uneven constant depth levels of $z = -h_1$ and $z = -h_3$ with $h_3 < h_1$. The flexible porous breakwater is fixed at $z = -h_3$ at $x = L + L_1$ with and without wall on the lee side. According to the geometry of problem, whole fluid region is divided into four sub-regions as shown in Figure 1. The first region is defined as $\Omega_I = \{-\infty < x < 0, -\infty < y < \infty, -h_1 \leq z \leq 0\}$, second region is $\Omega_{II} = \{0 \leq x \leq L, -\infty < y < \infty, -h_2(x) \leq z \leq 0\}$, third region is $\Omega_{III} = \{L \leq x \leq L + L_1, -\infty < y < \infty, -h_3 \leq z \leq 0\}$ and the last region is $\Omega_{IV} = \{L + L_1 \leq x \leq \infty, -\infty < y < \infty, -h_3 \leq z \leq 0\}$ for scattering problem and $\Omega_{IV} = \{L + L_1 \leq x \leq L + L_1 + W, -\infty < y < \infty, -h_3 \leq z \leq 0\}$ for trapping problem. The fluid in each region is assumed to be inviscid, incompressible and the

motion is irrotational and wave motion is assumed to be simple harmonic in time with angular frequency ω . With all these assumptions, fluid motion can be described in terms of velocity potential, $\Phi_r = \text{Re}\{\phi_r e^{-i(\mu_y y + \omega t)}\}$ for $r = \text{I, II, III, IV}$ with $i = \sqrt{-1}$ and $\mu_y = \beta_0 \sin \theta$, where β_0 being the wave-number of incident wave.

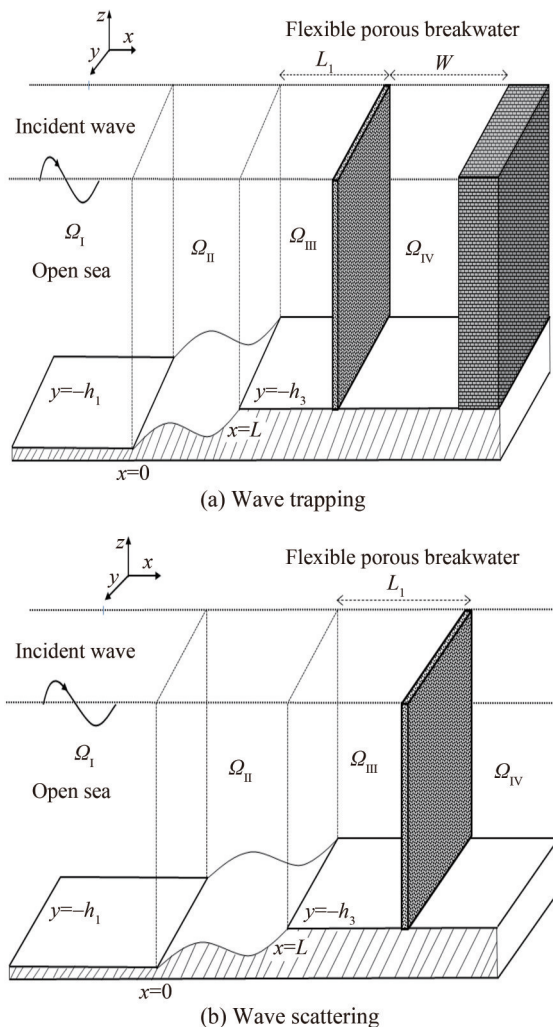


Figure 1 Depiction of wave trapping and scattering by a flexible porous breakwater in water of undulating bottom

The spatial velocity potential ϕ_r for $r = \text{I, II, III, IV}$ satisfy the Helmholtz equation

$$\left(\frac{\partial^2}{\partial x^2} + \frac{\partial^2}{\partial z^2} - \mu_y^2\right)\phi_r = 0 \text{ for } r = \text{I, II, III, IV} \quad (1)$$

In addition, ϕ_r has to satisfy the free-surface boundary condition in open water region:

$$\frac{\partial \phi_r}{\partial z} - \mathcal{K}\phi_r = 0 \text{ on } z = 0, r = \text{I, II, III, IV} \quad (2)$$

where $\mathcal{K} = \omega^2/g$ and g is the gravitational constant. Now, boundary condition on flat bottom is given by

$$\frac{\partial \phi_r}{\partial z} = 0 \text{ on } z = -h_1, -h_3, r = \text{I, III, IV} \quad (3)$$

whilst the boundary condition on varying bottom yields

$$\frac{\partial \phi_{\text{II}}}{\partial z} + \frac{dh_2}{dx} \frac{\partial \phi_{\text{II}}}{\partial x} = 0 \text{ on } z = -h_2 \quad (4)$$

Conditions at the interfaces between flat and varying bottom are given by

$$\phi_{\text{I}} = \phi_{\text{II}} \text{ at } x = 0 \quad (5)$$

$$\phi_{\text{II}} = \phi_{\text{III}} \text{ at } x = L \quad (6)$$

The continuity of velocity at the interface of porous breakwater is given as

$$\frac{\partial \phi_{\text{III}}}{\partial x} = \frac{\partial \phi_{\text{IV}}}{\partial x} \text{ at } x = L + L_1 \quad (7)$$

and boundary condition at $x = L + L_1$ for porous barrier yields

$$\frac{\partial \phi_r}{\partial x} = i\beta_0 G(\phi_{\text{III}} - \phi_{\text{IV}}) - i\omega\zeta \text{ at } x = L + L_1 \quad (8)$$

for $r = \text{III, IV}$. Here, porous effect parameter denoted by $G = \epsilon_s / (\beta_0 d_s (f_s - i s_s))$ is a complex number where ϵ_s is the porosity of barrier, d_s is thickness of porous barrier, f_s is the resistance force coefficient and s_s is the inertial force coefficient. The motion of porous plate is analyzed in two-dimensional as it is supposed to be uniform in the longitudinal direction. Further, plate deflection is assumed to small as compared to water depth and displacement of flexible plate in horizontal direction is measured with $\chi(y, z, t) = \text{Re}\{\zeta(z) e^{-i(\mu_y y + \omega t)}\}$ where $\zeta(z)$ is the complex deflection amplitude. Thus, the equation of motion for flexible plate acted upon by fluid pressure is given by

$$EI \left(\frac{d^2}{dz^2} - \mu_y^2\right)^2 \zeta + Q \left(\frac{d^2}{dz^2} - \mu_y^2\right) \zeta - m_s \omega^2 \zeta = i\omega\rho(\phi_{\text{III}} - \phi_{\text{IV}}) \text{ at } x = L + L_1 \quad (9)$$

where flexural rigidity is denoted by EI , Q represents the uniform compressible force acting on porous plate, $m_s = \rho_s d_s$ refers to the uniform mass per unit length with ρ_s is material density of flexible plate and d_s denotes the thickness of porous plate which is assumed to be small, ρ being the density of water. The porous plate is assumed to be fixed at the lower end. Hence, vanishing of the plate deflection and slope of deflection at the edge ($z = -h_3$) are given by

$$\zeta = 0 \text{ and } \zeta' = 0 \text{ at } x = L + L_1 \quad (10)$$

At the other end of porous plate, free edge conditions yield

$$\left(\frac{d^2}{dz^2} - \nu\mu_y^2\right)\zeta = 0 \text{ at } z = 0 \tag{11}$$

$$\left\{EI\left(\frac{d^2}{dz^2} - (2 - \nu)\mu_y^2\right)\frac{d}{dz} + Q\frac{d}{dz}\right\}\zeta = 0 \text{ at } z = 0 \tag{12}$$

where ν being the Poisson’s ratio of flexible breakwater. Next, no-flow condition towards the wall is given as

$$\frac{\partial\phi_{IV}}{\partial x} = 0 \text{ at } x = L + L_1 + W \tag{13}$$

Finally, far-field conditions in the region Ω_1 and Ω_{IV} are given by

$$\phi_I = (I_0 e^{ip_0 x} + R_0 e^{-ip_0 x}) \frac{ig \cosh\beta_0(z + h_1)}{\omega \cosh\beta_0 h_1} \text{ as } x \rightarrow -\infty \tag{14}$$

$$\phi_{IV} = T_0 e^{iq_0 x} \frac{ig \cosh\gamma_0(z + h_3)}{\omega \cosh\gamma_0 h_3} \text{ as } x \rightarrow \infty \tag{15}$$

where $p_0 = \sqrt{\beta_0^2 - \mu_y^2}$ and $q_0 = \sqrt{\gamma_0^2 - \mu_y^2}$ and, I_0 is known and R_0, T_0 are unknown constants associated with the amplitude of incident, reflected and transmitted waves respectively in regions Ω_1 and Ω_{IV} .

3 Method of solution

To tackle the solution to the present problem, eigenfunction expansion method is used in the region of constant depth, and a modified mild-slope equation (Chamberlian and Porter, 1995) for oblique wave is applied in the region of the varying bottom. To achieve the full solution, the velocity potential for constant water depth is matched with the MMSE. The bottom profile from $0 < x < L$ is assumed to be continuous and may have slope discontinuity at $x = 0$ and $x = L$. To handle these slope discontinuity, mass conserving jump conditions are applied at $x = 0$ and $x = L$ (Porter and Staziker, 1995). The velocity potential ϕ_I in the region Ω_I is expanded as

$$\phi_I(x, z) = \{I_0 e^{ip_0 x} + R_0 e^{-ip_0 x}\}U_0 + \sum_{n=1}^{\infty} R_n e^{-ip_n x} U_n \tag{16}$$

where I_0 is a known constant associated with the amplitude of the incident wave and R_n represents the unknown amplitudes of the reflected wave. Here, $U_n = (ig/\omega) \cosh\beta_n(z + h_1)/\cosh\beta_n h_1$ are the vertical eigenfunctions and $p_n = \sqrt{\beta_n^2 - \mu_y^2}$ for $n = 0, 1, 2, \dots, N$. Here, β_n is a positive real zero for $n = 0$ and a purely imaginary zero for $n = 1, 2, 3, \dots, N$ of the

dispersion equation $\beta \tanh\beta h_1 - \mathcal{K} = 0$ in β . Further, the velocity potential ϕ_{II} in the region Ω_{II} is written as Galerkin series

$$\phi_{II} = \sum_{n=0}^{\infty} \psi_n V_n(h_2, z) \tag{17}$$

where $\psi_n(x)$ are unknown functions and $V_n(h_2, z) = (ig/\omega) \cosh k_n(z + h_2)/\cosh k_n h_2$, $h_2(x)$ is the water depth and $k_n = k_n(x)$ being the local wave numbers for $n = 0, 1, 2, \dots$. The number of roots of dispersion equation $k \tanh kh_2 - \mathcal{K} = 0$ are infinite among which one is real and others are purely imaginary. The vertical eigenfunction $V_n(h_2, z)$ is taken from the region of the flat bottom which is similar to that in Eq. (16). This is the basic key assumption for the development of the mild-slope equation. Next, velocity potential ϕ_{III} and ϕ_{IV} in the regions Ω_{III} and Ω_{IV} respectively, are given as

$$\phi_{III} = \sum_{n=0}^{\infty} (A_n e^{iq_n x} + B_n e^{-iq_n x}) Z_n \tag{18}$$

$$\phi_{IV} = \sum_{n=0}^{\infty} T_n \cos q_n(x - (L + L_1 + W)) Z_n \tag{19}$$

when wall is present.

$$\phi_{IV} = \sum_{n=0}^{\infty} T_n e^{iq_n x} Z_n \tag{20}$$

for the case of wave scattering. $Z_n = (ig/\omega) \cosh\gamma_n(z + h_3)/\cosh\gamma_n h_3$ with $q_n = \sqrt{\gamma_n^2 - \mu_y^2}$ for $n = 0, 1, 2, \dots$. Here A_n, B_n and T_n are unknown constant and $\gamma_n (n = 0, 1, 2, \dots)$ are roots of dispersion equation $\gamma \tanh\gamma h_3 - \mathcal{K} = 0$. It is noted that the infinite series are truncated after N to obtain the solution. Further, the unknown function ψ_n in region Ω_{II} as in Eq. (17), satisfies the MMSE (as in Kaligatla et al. (2017)).

$$\frac{d}{dx} \left(a_n \frac{d\psi_n}{dx} \right) + (k_n^2 - \mu_y^2) a_n \psi_n + \sum_{m=0}^N \left[(b_{mn} - b_{nm}) \times \frac{dh_2}{dx} \frac{d\psi_m}{dx} + \left\{ b_{mn} \frac{d^2 h_2}{dx^2} + c_{mn} \left(\frac{dh_2}{dx} \right)^2 \right\} \psi_m \right] = 0 \tag{21}$$

where

$$a_n(h_2) = \int_{-h_2}^0 V_n^2 dz, \quad b_{mn}(h_2) = \int_{-h_2}^0 V_n \frac{\partial V_m}{\partial h_2} dz, \\ c_{mn}(h_2) = \frac{db_{mn}}{dh_2} - \int_{-h_2}^0 \frac{\partial V_m}{\partial h_2} \frac{\partial V_n}{\partial h_2} dz$$

for $n = 0, 1, 2, \dots, N$. Eq. (21) can be solved numerically

by selecting the different bottom profiles. Further, continuity of pressure at the interface boundaries are given by

$$\begin{cases} \psi_0(x) = I_0 e^{ip_0 x} + R_0 e^{-ip_0 x} \\ \psi_n(x) = R_n e^{-ip_n x} \end{cases} \text{ at } x = 0^+, n = 1, 2, \dots, N \quad (22)$$

and

$$\psi_n(x) = A_n e^{iq_n x} + B_n e^{-iq_n x} \text{ at } x = L, \text{ for } n = 0, 1, 2, \dots, N \quad (23)$$

In addition, mass conserving jump condition at these interface boundaries at $x = 0$ are derived as

$$a_0 \frac{d\psi_0}{dx} + ip_0 a_0 \psi_0 + h_2 \sum_{m=0}^N b_{m0} \psi_m = 2ip_0 a_0 I_0, \text{ for } n = 0 \quad (24)$$

$$a_n \frac{d\psi_n}{dx} + ip_n a_n \psi_n + h_2 \sum_{m=0}^N b_{mn} \psi_m = 0 \text{ for } n = 1, 2, \dots, N \quad (25)$$

and at $x = L + L_1$

$$\begin{aligned} a_n \frac{d\psi_n}{dx} - iq_n a_n \psi_n + h_2 \sum_{m=0}^N b_{mn} \psi_m \\ = -2iq_n q_n B_n e^{-iq_n x} \text{ at } x = L^-, n = 0, 1, 2, \dots, N \end{aligned} \quad (26)$$

Next, complex amplitude of structural displacement of breakwater is derived by using Eq. (18) and (19) into Eq. (9)

$$\begin{aligned} \zeta(z) = & \frac{\cosh N_0 z}{\cosh N_0 h_3} D_1 + \frac{\sinh N_0 z}{\sinh N_0 h_3} D_2 \\ & + \frac{\cos N_1 z}{\cos N_1 h_3} D_3 + \frac{\sin N_1 z}{\sin N_1 h_3} D_4 \\ & + M_0 \sum_{n=0}^N (A_n e^{iq_n x} + B_n e^{-iq_n x} - T_n \cos q_n (x - (L + L_1 + W))) \\ & \times \frac{\cosh \gamma_n (z + h_3)}{\cosh \gamma_n h_3} \end{aligned} \quad (27)$$

where D_1, D_2, D_3 and D_4 are arbitrary unknown constant and, $M_0 = ip\omega / (EI(\gamma_n^2 - \mu_y^2)^2 + Q(\gamma_n^2 - \mu_y^2) - m_s \omega^2)$ and N_0, N_1 are roots of equation $EI(x^2 - \mu_y^2)^2 + Q(x^2 - \mu_y^2) - m_s \omega^2 = 0$ in x . Upon utilising the fixed conditions by Eq. (10) at the bottom of breakwater at $x = L + L_1$ yields

$$\begin{aligned} D_1 - D_2 + D_3 - D_4 \\ + M_0 \sum_{n=0}^N (A_n e^{iq_n(L+L_1)} + B_n e^{-iq_n(L+L_1)} - T_n \cos q_n W) \frac{1}{\cosh \gamma_n h_3} = 0 \end{aligned} \text{ at } z = -h_3 \quad (28)$$

and

$$\begin{aligned} -N_0 \tanh N_0 h_3 D_1 + N_0 \coth N_0 h_3 D_2 \\ + N_1 \tan N_1 h_3 D_3 + N_1 \cot N_0 h_3 D_4 = 0 \text{ at } z = -h_3 \end{aligned} \quad (29)$$

Further, by using free edge conditions in Eqs. (11) and (12) at $z = 0$

$$\begin{aligned} \frac{N_0^2 - \nu \mu_y^2}{\cosh N_0 h_3} D_1 - \frac{N_1^2 + \nu \mu_y^2}{\cos N_1 h_3} D_3 \\ + M_0 \sum_{n=0}^N \left((\gamma_n^2 - \nu \mu_y^2) (A_n e^{iq_n(L+L_1)} + B_n e^{-iq_n(L+L_1)} \right. \\ \left. - T_n \cos q_n W) \right) = 0 \end{aligned} \quad (30)$$

and

$$\begin{aligned} \frac{EIN_0^3 + (Q - EI(2 - \nu)\mu_y^2)N_0}{\sinh N_0 h_3} D_2 \\ - \frac{EIN_1^3 - (Q - EI(2 - \nu)\mu_y^2)N_1}{\sin N_1 h_3} D_4 \\ + M_0 \sum_{n=0}^N \left((EI\gamma_n^3 + (Q - EI(2 - \nu)\mu_y^2)\gamma_n) (A_n e^{iq_n(L+L_1)} \right. \\ \left. + B_n e^{-iq_n(L+L_1)} - T_n \cos q_n W) \tanh \gamma_n h_3 \right) = 0 \end{aligned} \quad (31)$$

Now, by using the boundary conditions Eqs. (7) and (8) at the interface $x = L + L_1$ are given as

$$\sum_{n=0}^N (iA_n e^{iq_n(L+L_1)} - iB_n e^{-iq_n(L+L_1)} - T_n \sin q_n W) X_{mn} = 0 \quad (32)$$

and

$$\begin{aligned} \omega \int_{-h_3}^0 \frac{\cosh N_0 z}{\cosh N_0 h_3} dz D_1 + \omega \int_{-h_3}^0 \frac{\sinh N_0 z}{\sinh N_0 h_3} dz D_2 \\ + \omega \int_{-h_3}^0 \frac{\cos N_1 z}{\cos N_1 h_3} dz D_3 + \omega \int_{-h_3}^0 \frac{\sin N_1 z}{\sin N_1 h_3} dz D_4 \\ + \sum_{n=0}^N \left\{ (q_n - \beta_0 G + \omega M_0) A_n e^{iq_n(L+L_1)} \right. \\ \left. - (q_n + \beta_0 G - \omega M_0) B_n e^{-iq_n(L+L_1)} \right. \\ \left. + (\beta_0 G - M_0 \omega) T_n \cos q_n W \right\} X_{mn} = 0 \end{aligned} \quad (33)$$

where $X_{mn} = \int_{-h_3}^0 Z_n Z_m dz$. The system of Equations (22)–(26) along with (28)–(33) can be solved numerically by using matrix method.

4 Results and discussion

In this section, numerical results are computed in MATH-EMATICA to analyze the effect of porosity and flexibility

of breakwater in the interaction of waves with a breakwater in the presence of step-type bottom. The modified mild-slope equation is solved by using the in-built function NDSolve and the system of algebraic equations from Eqs.(22)–(25) along with (27)–(32) are computed numerically in MATHEMATICA. To validate the model, we have matched with the result of Krishnendu and Balaji (2020) and Behra et al. (2015) in the less general case of $h_3/h_1 \rightarrow 1$ for non-flexible breakwater for the case of trapping problem. The model is analyzed for the plane sloping bottom bed, rippled bottom, concave up and concave down type bottom as shown in Figure 2. In region Ω_1 , a fixed wavelength of plane gravity wave $\lambda_1 = 2\pi/\beta_0$ is used to denote physical parameters in non-dimensional form. Few parameters are fixed such as amplitude of incident wave $I_0 = 1$, acceleration due to gravity $g = 9.81 \text{ m/s}^2$, length of varying bottom $L/\lambda_1 = 1$, distance between varying bottom and breakwater $L_1/\lambda_1 = 0.4$, distance between breakwater and wall $W/\lambda_1 = 1$, angle of incident wave $\theta = 30^\circ$, depth ratio $h_3/h_1 = 0.5$, $\gamma_s = \frac{EI}{\rho h_3^4} = 0.1$, $m_s = 10$, $\nu = 0.3$ are kept fixed until it is mentioned. The compressible force Q of flexible breakwater is assumed to be zero throughout the numerical computation. The non-dimensional reflection coefficient K_r , and transmission coefficient K_t is given by

$$K_r = \left| \frac{R_0}{I_0} \right|, \quad K_t = \left| \frac{\gamma_0 \tanh \gamma_0 h_3 T_0}{\beta_0 \tanh \beta_0 h_3 I_0} \right| \quad (34)$$

respectively, and non-dimensional wave force on breakwater K_f and force on wall K_w are derived as

$$K_f = \left| \frac{-i\omega}{gh_1^2} \int_{-h_3}^0 (\phi_{IV}(x, z) - \phi_{III}(x, z)) dz \right|,$$

$$K_w = \left| \frac{-i\omega}{gh_1^2} \int_{-h_3}^0 (\phi_{IV}(x, z)) dz \right| \quad (35)$$

respectively. The bottom profiles used in this study are given by

$$\begin{cases} h_1 - (h_1 - h_3) \left\{ 1 - \alpha \left(1 - \frac{x}{L} \right)^2 + (\alpha - 1) \left(1 - \frac{x}{L} \right) \right\} \\ h_3 + (h_1 - h_3) \left\{ 1 + 2 \left(\frac{x}{L} \right)^3 - 3 \left(\frac{x}{L} \right)^2 - d \left(1 - \cos \frac{2s\pi x}{L} \right) \right\} \end{cases}$$

for $0 < x < L$ (36)

In the given Eq. (36), first bottom profile is used for plane sloping bottom, concave-up and concave-down type bottom whereas second bottom profile is used for sinusoidal bottom. The parameter α used in bottom profiles determines the shape of bottom such as $\alpha = 0$ renders to plane sloping

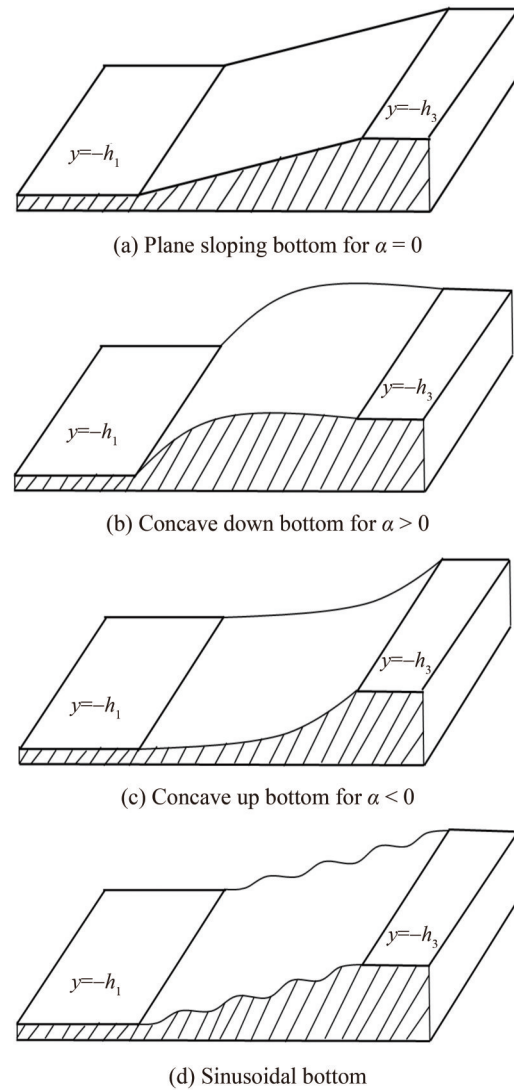


Figure 2 Bottom Profiles of seabed

bottom, $\alpha > 0$ provides concave down type bottom and $\alpha < 0$ corresponds to concave up type bottom. Also, second bottom profile in Eq. (36) is used for rippled type bottom, here d refers to ripple amplitude and $L = sl$, where l is the wavelength of rippled bottom and s denotes the number of ripples present in the bottom.

4.1 Wave trapping

In this subsection, the case of presence of impermeable wall at distance W from porous flexible breakwater is discussed. Here, effect of bottom topography and wave absorbing nature of breakwater have been studied assuming rigid impermeable wall present in front of breakwater. Thus, we present reflection coefficient K_r , wave force on breakwater K_f and wall K_w when wave interacts with porous flexible breakwater in the presence of bottom undulation.

To validate the present model, the experimental results

of Krishnendu and Balaji (2020) (Figure 9(a)) concerned with the trapping of normal wave incidents are compared with the present model as shown in Figure 3(a). In this figure, continuous lines represent the present theoretical results whereas discrete points are used to show the experimental results obtained in Krishnendu and Balaji (2020). The parametric values used in this figure are $\alpha = 0, \theta = 0^\circ, W = 1$ and $\gamma_s = 1$. It is to noted that When $h_3/h_1 \rightarrow 1$ then step type bottom is converted to flat bottom and for non-dimensional flexural rigidity $\gamma_s \geq 1$ (as in Koley et al. (2015)), breakwater works as non-flexible porous breakwater. Figure 3 is plotted to show the reflection coefficient, wave force on breakwater and wall as a function of chamber width W/λ_1 . The results from Krishnendu and Balaji (2020) obtained experimentally agrees well with the present theoretical estimates as shown in Figure 3(a). To ensure the accuracy of the present model, root mean square error (RMSE) is performed. It is found that RMSE for 20% porosity is 0.05, 15% porosity is 0.024, 10% porosity is 0.024 and 5% porosity is 0.034. This RMSE values show the very good match for accuracy of the present model. It is evident from Figure 3(a) that reflection is less for higher porosity and corresponding wave force on breakwater is less whereas wave force on wall is high. It is evident from Figure 3(b) that wave force on breakwater decreases continuously with respect to non-dimensional distance between wall and porous breakwater W/λ_1 . Figure 4 is plotted to illustrates the variation of reflection coefficient as a function of chamber length W/λ_1 . The numerical values of parameters are taken as $\beta_0 h_1 = 1.3, \alpha = 0, f_s = 5, \epsilon_s = 0.3, s_s = 1$ and $d_s/h_1 = 0.05$. Particularly, in Figure 4(a), the present problem is compared with the Figure 8 of Liu et al. (2007) concerning to wave trapping by thin porous breakwater in the presence of uniform bottom ($h_3/h_1 = 0.99$). It is found that present result matches exactly with the plot of Liu et al. (2007) in Figure 4(a). It is to noted that for flexural rigidity $\gamma_s = 1$, breakwater becomes non flexible and act as only porous without flexibility. In Figure 4(a), dotted line represents the result of Liu et al. (2007) when breakwater is assumed to be only porous and flexibility is absent ($\gamma_s = 1$). Moreover, when water depth ratio is varying, reflection coefficient increases as depth ratio decreases and periods of oscillations reduces which leads to shift in minima. In Figure 4(b), effect of flexural rigidity γ_s is studying when length of chamber is varying on x -axis with $h_3/h_1 = 0.35$. It is observed that least reflection is observed for $\gamma_s = 0.002$ and high reflection occurs for $\gamma_s = 0.0002$ due to much flexibility in breakwater. Hence, moderate values of flexural rigidity is preferable to attained tranquil region.

In Figure 5, reflection coefficient K_r , wave force acting on breakwater K_f and wall K_w versus non-dimensional length of varying bottom is plotted to study the effect of flexural rigidity γ_s . The numerical values of parameters used in this figure are $T = 8$ s, $h_3/h_1 = 0.25, G = 1 + i, W/\lambda_1 = 0.4$ and

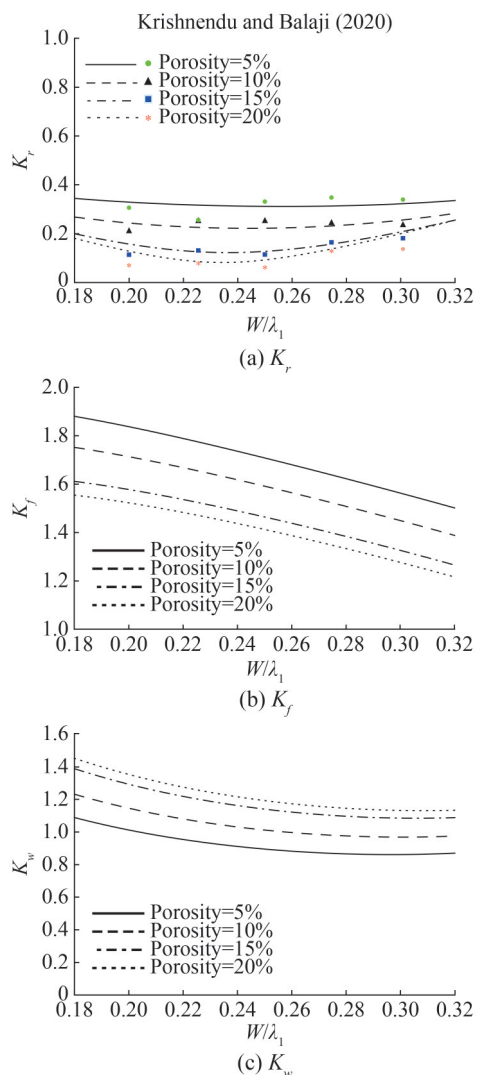


Figure 3 Reflection coefficient K_r , force on breakwater K_f and force on wall K_w versus non-dimensional length W/λ_1 for different porosity with $T = 2.0$

$\alpha = 1$. A comparison of the present study is made in this figure with Behera et al. (2015) (Figure 3(a)) in which they analyzed wave interaction of non-flexible breakwater placed in front of an impermeable wall in the presence of step type bottom. The solid line represents the result of Behera et al. (2015) in Figure 5(a). It is observed from Figure 5(a) that higher reflection is observed for $\gamma_s = 1$ which may be due to rigid porous breakwater also, higher reflection is observed for $\gamma_s = 0.0002$ as it allows more water to pass due to much flexibility of breakwater and reflected by impermeable wall for the smaller length of varying bottom. On the other hand, less wave force is exerted on breakwater for smaller values of varying bottom and higher wave force is noticed on wall for $\gamma_s = 0.0002$ which is evident from Figures 5(b) and 5(c) respectively. From Figure 5, it is concluded that less reflection is observed in the case of $\gamma_s = 0.0001$ for $L/\lambda_1 \geq 0.4$ and more wave force exerts on breakwater which results in less wave force on the wall.

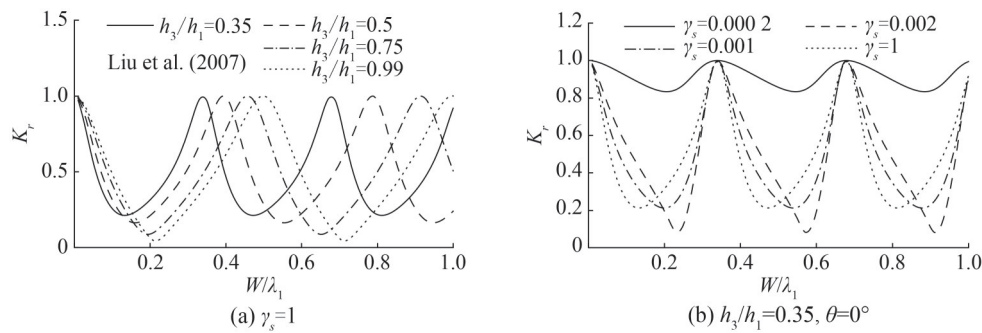


Figure 4 Reflection coefficient K_r versus non-dimensional length W/λ_1 for different values of depth ratio h_3/h_1 with $\gamma_s = 1$, and for different values of flexural rigidity γ_s with $h_3/h_1 = 0.35$ and $\theta = 0^\circ$

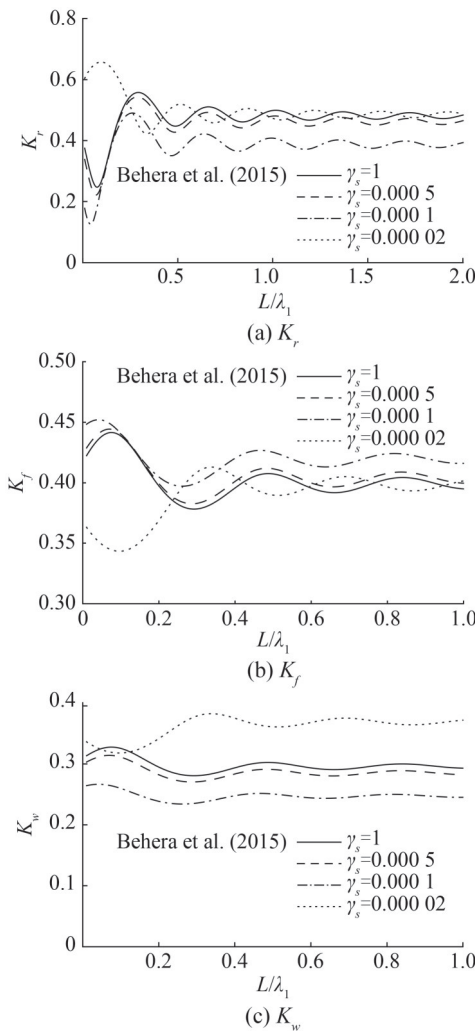


Figure 5 Reflection coefficient K_r , force on breakwater K_f and force on wall K_w versus non-dimensional length L/λ_1 for different values of γ_s

Figure 6 shows the variation of reflection coefficient K_r , wave force acting on breakwater K_f and wall K_w versus non-dimensional length of a varying bottom for the different bottom profile as defined in Figure 2. The numerical values of parameters are same as in Figure 5. A similar pattern is observed for concave down, plane sloping and concave up type bottom. Further, the oscillatory pattern of these bottom

profiles vanishes with increasing length of varying bottom L/λ_1 . Figure 6 shows that rippled bottom profile exhibits higher reflection and least waves transmitted through breakwater for the smaller length of varying bottom which causes less wave force exerting on the impermeable wall which may be a favorable situation to protect the harbor regions.

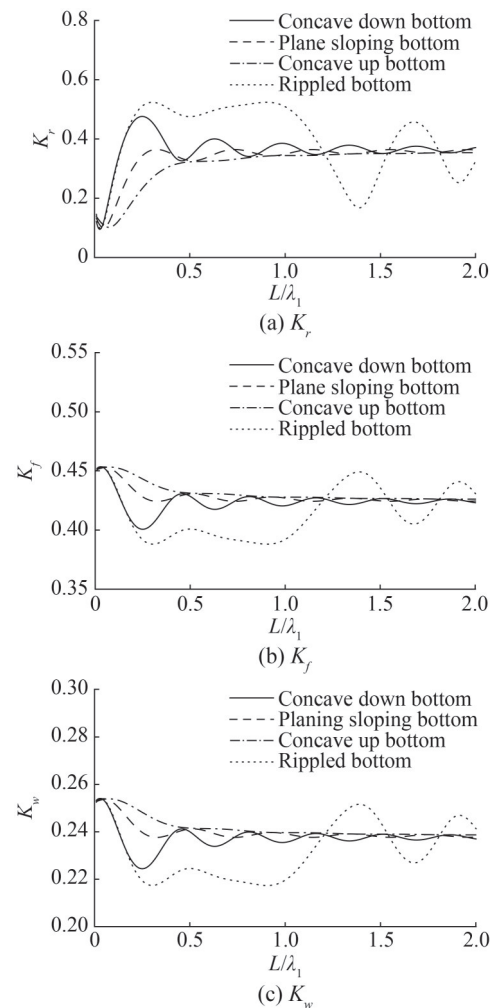


Figure 6 Reflection coefficient K_r , force on breakwater K_f and force on wall K_w versus non-dimensional length L/λ_1 for different bottom profiles with flexural rigidity $\gamma_s = EI/\rho h_3^3 = 0.02$

Figure 7 is plotted to examine the changes in reflection coefficient K_r , wave force acting on breakwater K_f and wall K_w for different values of depth ratio h_3/h_1 when non-dimensional wavenumber is varying on the x -axis. An oscillatory trend is observed with respect to wave number. Higher reflection occurs for flat bottom ($h_3/h_1 = 0.99$) and amplitude of oscillation in reflection increases as depth ratio decreases. On the other hand, Force on breakwater and wall decreases as the wavenumber increases on x -axis as observed in Figures 7(b) and (c). Hence, shallow water waves exert high wave force on the breakwater as well as on wall. Also, as the depth ratio decreases wave force on wall decreases with more minima.

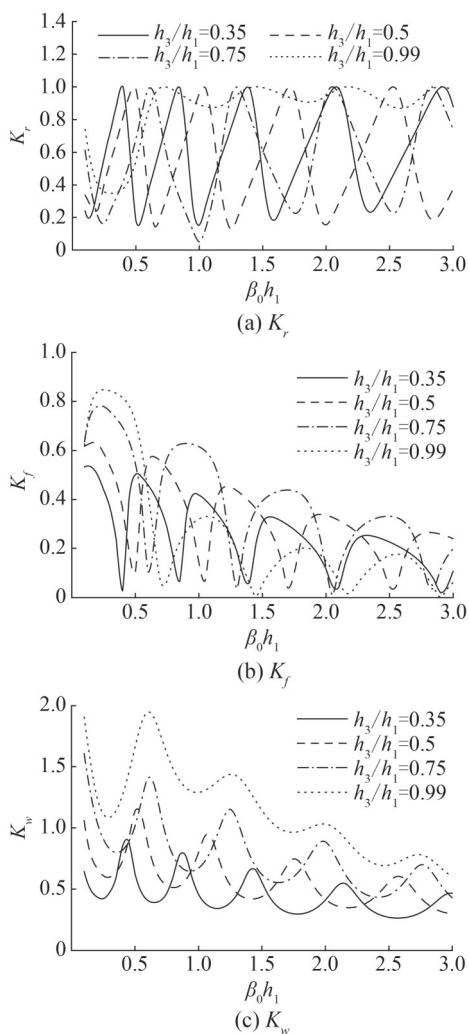


Figure 7 Reflection coefficient K_r , force on breakwater K_f and force on wall K_w versus non-dimensional wavenumber $\beta_0 h_1$ for different values of depth ratio h_3/h_1

In Figure 8, reflection coefficient K_r , wave force acting on breakwater K_f and wall K_w are studied as a function of the distance between breakwater and wall for different values of depth ratio h_3/h_1 . These coefficients are found to be periodic with respect to the length of chamber width. Parametric

values used in this figure are $G = 1 + i$, $\beta_0 h_1 = 1$, $\lambda_s = 0.01$ and $\alpha = 0$. From Figure 8(a), it is observed that the least wave is reflected for the depth ratio $h_3/h_1 = 0.75$ which results in high force on breakwater as in Figure 8(b). The presence of flat bottom causes high wave force on wall and the least wave force exert on the wall due to smaller values of depth ratio. It is also observed that the number of minima increases with a decrease in depth ratio. A drift towards left side in minima of wave force on wall is noticed in Figure 8(c) for decreasing depth ratio h_3/h_1 .

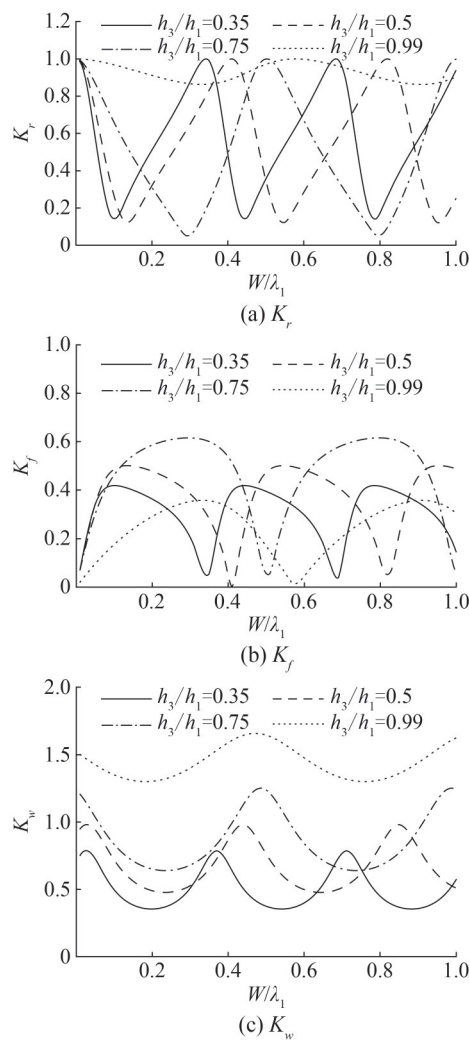


Figure 8 Reflection coefficient K_r , force on breakwater K_f and force on wall K_w versus non-dimensional chamber length W/λ_1 for different values of depth ratio h_3/h_1

Figure 9 demonstrates the effect of chamber width W/λ_1 on reflection coefficient, wave force on breakwater and wall for different values of flexural rigidity γ_s . The numerical values of parameters used in this figure are chosen as $G = 1 + i$, $\beta_0 h_1 = 1$ and $\alpha = 0$. It is observed that wave reflection and wave force on the wall is high for smaller values of flexural rigidity γ_s . Figure 9(a) illustrates that maximum

reflection is achieved for certain chamber width W/λ_1 which implies minimum force attained on breakwater as in Figure 9(b). It is noted that for certain chamber width moderate values of flexural rigidity, substantial less wave force exerts on breakwater and wall.

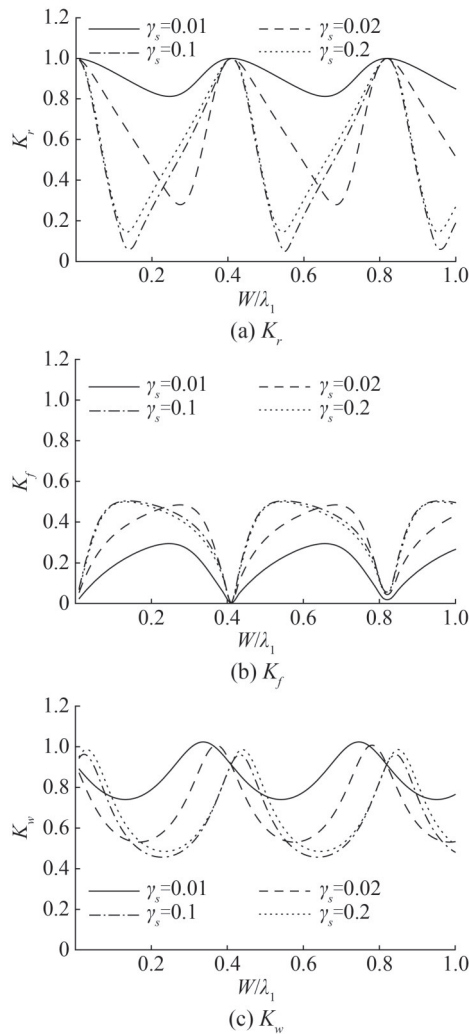


Figure 9 Reflection coefficient K_r , force on breakwater K_f and force on wall K_w versus non-dimensional chamber length W/λ_1 for different values of flexural rigidity $\gamma_s = E/I\rho h_3^4$

In Figure 10, reflection coefficient K_r , wave force on breakwater K_f and wall K_w are depicted against the angle of the incident for different values of depth ratio h_3/h_1 . The parameters chosen in this figure are $G = 1 + i$, $\beta_0 h_1 = 1$, $\alpha = 0$ and $\lambda_s = 0.01$. For the flat bottom ($h_3/h_1 = 0.99$), higher reflection occurs as shown in Figure 10(a) which causes higher wave force on the wall as observed from Figure 10(c). On the other hand, less reflection occurs for the depth ratio $h_3/h_1 = 0.35$ at an angle of incidence $\theta = 75^\circ$ which implies more energy dissipation as high wave force on wall and breakwater does not exert. It is to note that full reflection is achieved for a certain angle of the incident wave at which zero wave force exerts on the break-

water. however, wave force on the wall is increasing as depth ratio h_3/h_1 is increasing for the angle of incident $\theta \geq 65^\circ$.

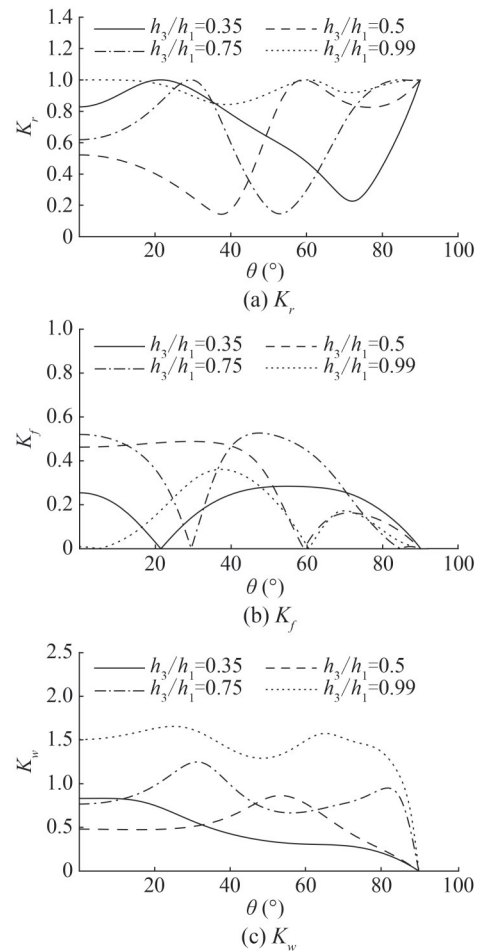


Figure 10 Reflection coefficient K_r , force on breakwater K_f and force on wall K_w versus angle of incident θ for different values of depth ratio h_3/h_1

Effect of different flexural rigidity on reflection coefficient K_r , wave force on breakwater K_f and wall K_w are studied in Figure 11 when the angle of incident wave is varying on x -axis. In Figure 11, a similar pattern is observed as in Figure 10 that for a certain range of angle of incident $50^\circ \leq \theta \leq 70^\circ$. Figure 11(a) demonstrates that the curve of reflection coefficient shows more oscillatory for the larger values of flexural rigidity γ_s . Also, it is to note that smaller values of flexural rigidity cause more deflection which result in less wave force on barrier and high wave force on the impermeable wall as observed in Figures 11(b) and 10(c) respectively.

In Figure 12, reflection coefficient K_r , wave force on breakwater K_f and wall K_w are illustrated with varying porous effect parameter G for different values of depth ratio h_3/h_1 . The numerical value of parameters are taken as $\alpha = 0$, $\theta = 30^\circ$, $\beta_0 h_1 = 1$, $\lambda_s = 0.01$ and $W/\lambda_1 = 1$. Figure 12(a) depicts that there is large variation in reflection coefficient for porosity $0 \leq G \leq 2$ and maximum reflection occurs for

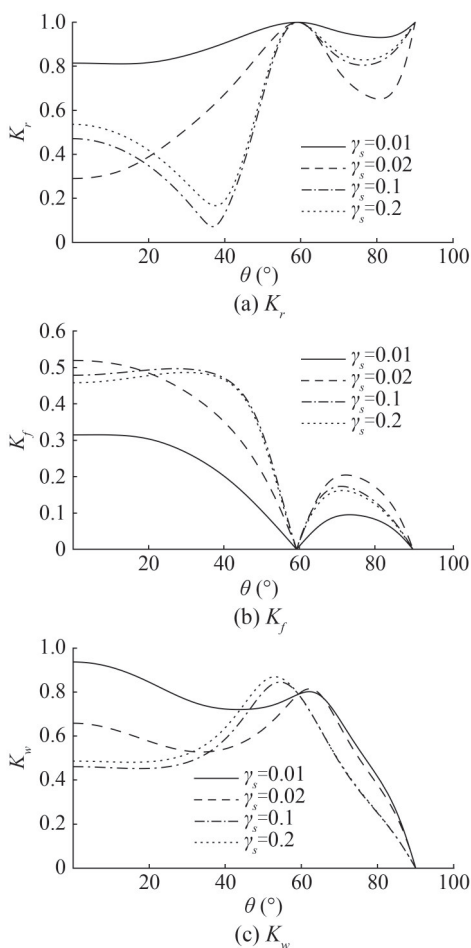


Figure 11 Reflection coefficient K_r , force on breakwater K_f and force on wall K_w versus angle of incident θ for different values of flexural rigidity $\gamma_s = EI/\rho h_3^4$

uniform bottom $h_3/h_1 = 0.99$. Initially, the reflection coefficient decreases sharply as G increases then it increases for larger values of G and does not alter its pattern beyond a certain value of G as shown in Figure 12(a). Smaller values of porous effect parameter ($G < 2$) cause less wave force is exerting on breakwater whereas force on wall is high for the uniform bottom. Figure 12(b) and (c) reveals that least wave force is acting on breakwater and wall for the depth ratio $h_3/h_1 = 0.35$. It is to note that wave energy is dissipated for $G = 1.25$ as the reflection coefficient is minimum at this point however there is no such variation in wave force on breakwater and wall. From these observations, porous effect parameter $0.5 < G < 2$ may be preferable for dissipating wave energy for smaller depth ratio $h_3/h_1 = 0.5$ and 0.35 .

Figure 13 is plotted to show the deflection of flexible porous plate ζ/h_1 against z/h_1 for different values of flexural rigidity γ_s and porous effect parameter G when the plate is fixed at the bottom edge. Some specific amount of parameters are fixed as $h_3/h_1 = 0.5$, $W/\lambda_1 = 1$, $\alpha = 0$, $\theta = 30^\circ$ and $\beta_0 h_1 = 1$. From Figure 13(a), the plate is much deflected

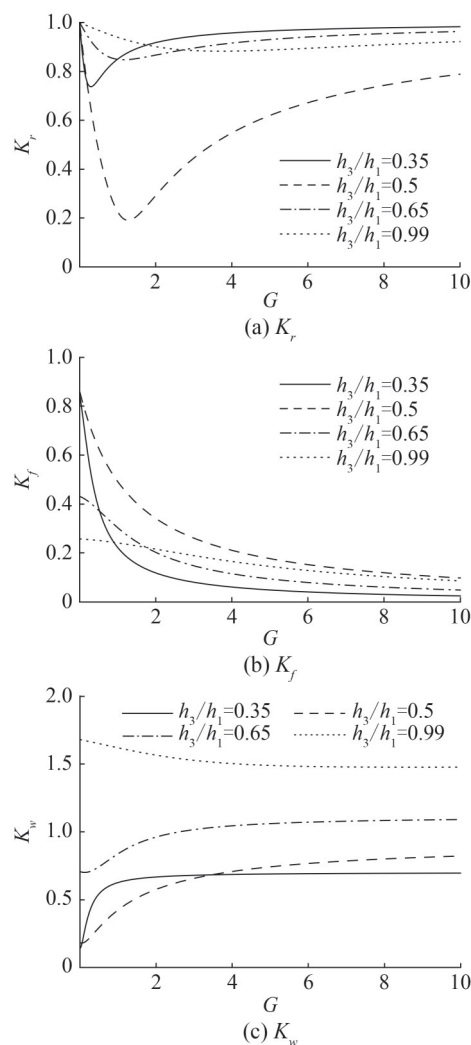


Figure 12 Reflection coefficient K_r , force on breakwater K_f and force on wall K_w versus porous effect parameter G for different values of depth ratio h_3/h_1

when flexibility γ_s is added to the breakwater which is an obvious phenomenon. Also for rigid breakwater $G = 0$, deflection is high as compared to porous flexible breakwater since it does not allow transmission of water as observed in Figure 13(b) which causes high wave force on breakwater as observed in Figure 12(b).

4.2 Wave scattering

In coastal regions or marinas, it is desirable to maintain healthy ecosystem and make harbour free from stagnating pollution. It is assumed that there are no fixed boundaries at far field, hence, in this subsection, we present scattering of waves by flexible porous breakwater in the presence of uneven bottom. In this case, a part of wave energy will be dissipated and some will be transmitted to lee side of breakwater. Thus, in this view point, we study reflection coefficient K_r and transmission coefficient K_t and wave force on wall K_w .

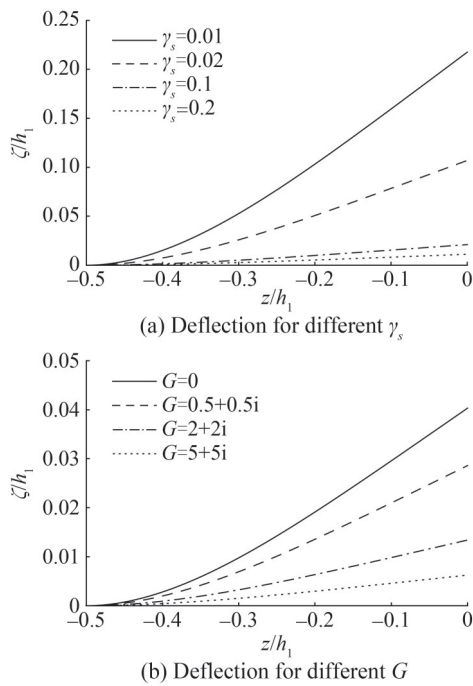


Figure 13 Plate deflection ζ/h_1 versus z/h_1 for different values of γ_s with $G = 1 + i$ and G with $\gamma_s = 0.1$

Figure 14 demonstrates the influence of various bottom profiles with varying horizontal bottom length L/λ_1 on reflection, transmission and wave force on breakwater. The used parameters to plot these graph are as $h_3/h_1 = 0.25$, $\gamma_s = 0.02$, $G = 1 + i$ and $T = 8$ s. The observation received in this plot is similar to the case of trapping of waves as in Figure 6. The result demonstrates that each type of bottom shows higher reflection and oscillatory pattern for smaller length of bottom and curves variation diminish as its length increases except for the case of rippled bottom. It is observed from Figure 14 that most of the wave energy is reflecting due to presence of rippled bottom for small length of varying bottom which leads to least transmission and hence least hydrodynamic force exerts on flexible breakwater.

Further, to analyze the effect of depth ratio h_3/h_1 and flexural rigidity γ_s of flexible porous breakwater on Bragg reflection which takes place in the presence of sinusoidal bottom. The phenomenon of Bragg resonance can be found in several articles such as Dalrymple and Kirby (1986), Tabssum et al. (2020) in the presence of structures. The ideal condition for Bragg resonance is $2l/\lambda_1 = 1$ at which reflection enhances significantly. In the present article, reflection and transmission coefficients K_r , K_t and wave load on porous breakwater K_f are studied in Figure 15 and Figure 16 as a function of frequency parameter $2l/\lambda_1$.

Figure 15 is presented to show the effect of depth ratio h_3/h_1 on Bragg scattering coefficients. The fixed parameters for this figure are as $G = 1 + i$, $\gamma_s = 0.02$, $L_1 = 10$, $s = 6$, $l = 6.4$ and $d = 0.08$. Figure 15(a) reveals that more Bragg resonance is pronounced near $2l/\lambda_1 = 0.75$ and reflection is

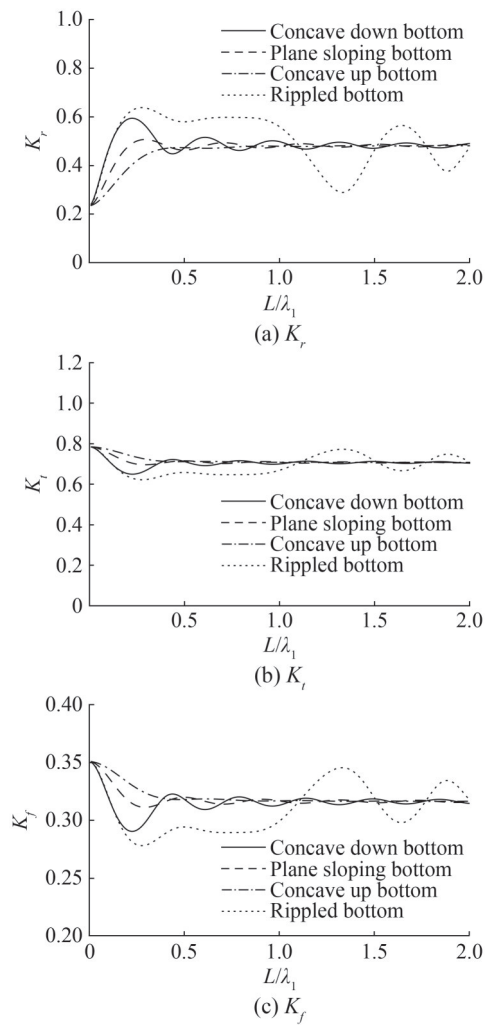


Figure 14 Reflection coefficient K_r , transmission coefficient K_t and force on breakwater K_f versus length of varying bottom L/λ_1 for different bottom profiles

high for depth ratio $h_3/h_1 = 0.35$. Moreover, reflection coefficient decreases as depth ratio increases and resonance peak shifts towards right. It is seen that least transmission occurs at $2l/\lambda_1 = 0.75$ which may be favourable condition for creating calm zone near harbour region but variation with respect to different depth ratio is negligible. However, significant variation is noticed with respect to depth ratio. Least hydrodynamic force is exerting on porous flexible breakwater for depth ratio $h_3/h_1 = 0.35$.

Figure 16 shows the influence of flexural rigidity γ_s on Bragg scattering coefficients. The parameters used to plot this figure are same as in Figure 15. From Figure 16(a), it exposes that least reflection is pronounced at $2l/\lambda_1 = 0.9$ for smaller values of flexural rigidity which leads to higher transmission and less wave force as in Figures 16(b) and (c) respectively. It is observed that higher wave energy dissipation occurs for larger values of frequency parameter as zero reflection and wave force on breakwater is observed whereas transmission is less less for $\gamma_s = 0.001$ and 0.002 .

In Figure 17, deflection of the flexible porous breakwater is shown for different values of flexural rigidity $\gamma_s = EI/\rho h h_1^4$ and porous effect parameter G . The parameters used in this plot are $\beta_0 h_1 = 1$, $\alpha = 0$, $\gamma_s = 0.1$ and $G = 1 + i$. From Figure 17(a), plate deflection is observed high for small values of flexural rigidity $\gamma_s = 0.01$ and less deflection for

higher values as noticed in Figure 13(a). Deflection decreases as flexural rigidity increases. In Figure 17(b), highest deflection occurs for impermeable breakwater for $G = 0$. However, deflection is less as compare to the case of trapping in Figure 13 which may be due to absence of impermeable wall.

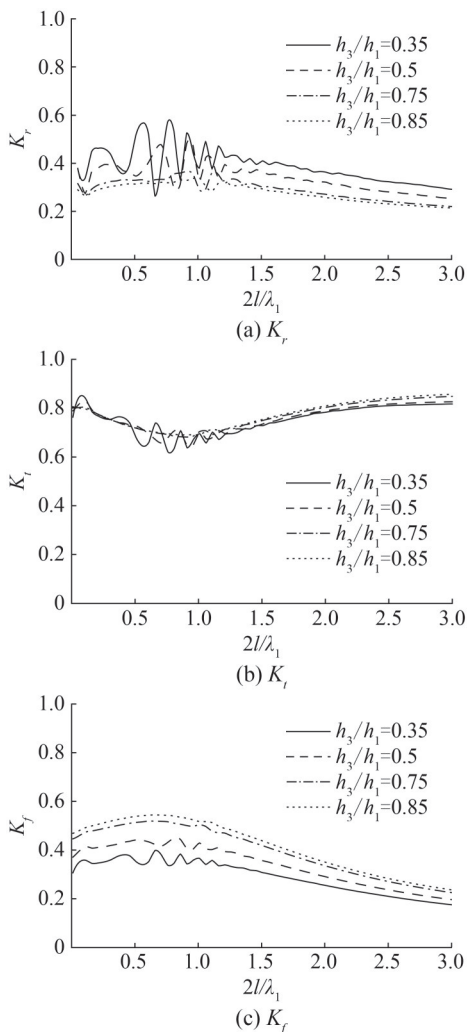


Figure 15 Reflection coefficient K_r , transmission coefficient K_t and force on breakwater K_f versus $2l/\lambda_1$ for different values of depth ratio h_3/h_1

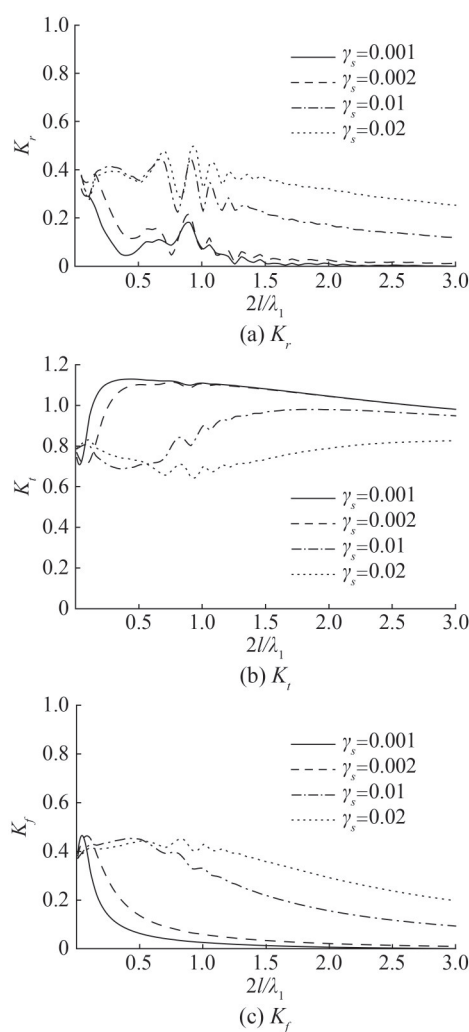


Figure 16 Reflection coefficient K_r , transmission coefficient K_t and force on breakwater K_f versus $2l/\lambda_1$ for different values of flexural rigidity γ_s

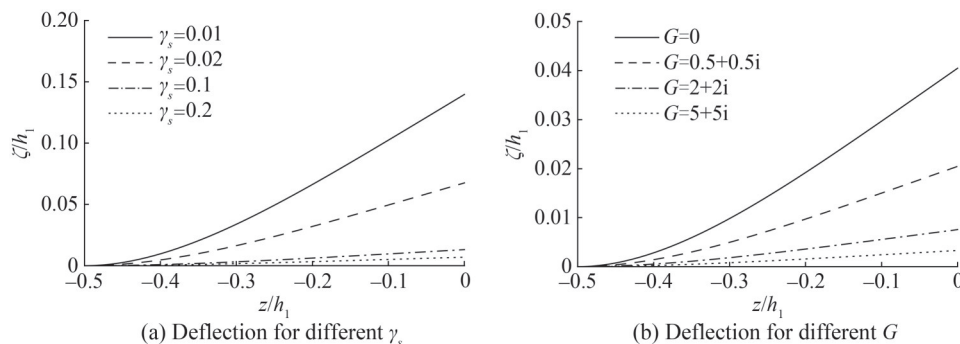


Figure 17 Plate deflection for different values of flexural rigidity $\gamma_s = EI/\rho h h_1^4$ and porous effect parameter G

5 Conclusions

In the present study, the effect of bottom variation on the trapping and scattering of obliquely incident waves is analyzed using a flexible porous breakwater. The study is carried out within the framework of linear water wave theory, and Darcy's law is used to model the flow past the porous breakwater. To solve the physical problem, an eigenfunction expansion in the region of uniform bottom is coupled with the mild-slope equation for step-type bottom topography. The system of equations is obtained by imposing suitable boundary conditions at the interface, and mass-conserving jump conditions are applied at the slope discontinuities on the bottom edge. The present theoretical model is compared with the result of Krishnendu and Balaji (2020) in less general case of porous breakwater in the presence of uniform bottom. Further, the results are validated with the plot of Behera et al. (2015) and Liu et al. (2007) in a limiting case.

The study reveals that wave reflection increases and minima drags towards left as depth ratio decreases. Additionally, minimum reflection occurs for flexural rigidity $\gamma_s = 0.002$. Further, the breakwater reflects less wave energy and exerts less wave force on the wall for intermediate values of the flexural rigidity γ_s . A large variation is observed for smaller values of the varying lengths of the bottom. However, a rippled type bottom profile may be more preferable for creating a tranquil environment, as it allows for more reflection and leads to the least force on the breakwater and wall for smaller lengths of varying bottom ($L/\lambda_1 < 1.25$). The oscillatory behavior of the reflection coefficient increases as the depth ratio decreases, and the amplitude of oscillation reduces as the non-dimensional wavenumber increases. For a particular distance between the breakwater and wall, and angle of incidence, negligible force is acting on the breakwater. It is observed that smaller values of the flexural rigidity of the breakwater result in less wave force on the breakwater and higher force on the wall for an angle of incidence $\theta > 60^\circ$. Moreover, due to the presence of a step-type bottom, complete reflection occurs for large values of G , and the force on the breakwater diminishes, resulting in the least force exerted on the wall. Plate deflection is more pronounced for smaller values of the porous effect parameter.

In the case of wave scattering, higher reflection is noticed for a rippled bottom with a smaller length of varying bottom. A smaller depth ratio allows for higher reflection and least transmission. Bragg resonance is pronounced at $2l/\lambda_1 = 0.75$, which may be a favorable case for a tranquil region near the harbor. Wave energy dissipation is higher for larger frequency parameters. Less deflection is observed in the case of scattering compared to wave trapping.

Competing interest All authors declare that there are no other competing interests.

References

- Behera H, Kaligatla RB, Sahoo T (2015) Wave trapping by porous barrier in the presence of step type bottom. *Wave Motion* 57: 219-230. <https://doi.org/10.1016/j.wavemoti.2015.04.005>
- Berkhoff JCW (1973) Computation of combined refraction diffraction. In *Proceedings of 13th International Conference on Coastal Engineering*, Vancouver, Canada, ASCE, 471-490. <https://doi.org/10.1061/9780872620490.027>
- Chamberlain PG, Porter D (1995) The modified mild-slope equation. *Journal of Fluid Mechanics* 291: 393-407. <https://doi.org/10.1017/S0022112095002758>
- Chwang AT (1983) A porous-wavemaker theory. *Journal of Fluid Mechanics* 132: 395-406. <https://doi.org/10.1017/S0022112083001676>
- Dalrymple RA, Kirby JT (1986) Water waves over ripples. *Journal of Waterway, Port, Coastal, and Ocean Engineering* 112(2): 309-319. [https://doi.org/10.1061/\(ASCE\)0733-950X\(1986\)112:2\(309\)](https://doi.org/10.1061/(ASCE)0733-950X(1986)112:2(309))
- Das S, Bora SN (2018) Oblique water wave damping by two submerged thin vertical porous plates of different heights. *Computational and Applied Mathematics* 37(3): 3759-3779. <https://link.springer.com/article/10.1007/s40314-017-0545-7>
- Gayen R, Mondal A (2014) A hypersingular integral equation approach to the porous plate problem. *Applied Ocean Research* 46: 70-78. <https://doi.org/10.1016/j.apor.2014.01.006>
- Gupta S, Naskar T, Gayen R (2022) Scattering of water waves by dual asymmetric vertical flexible porous plates. *Waves in Random and Complex Media*, 1-25. <https://doi.org/10.1080/17455030.2021.2022247>
- Kaligatla RB, Koley S, Sahoo T (2015) Trapping of surface gravity waves by a vertical flexible porous plate near a wall. *Journal of Applied Mathematics and Physics* 66(5): 2677-2702. <https://link.springer.com/article/10.1007/s00033-015-0521-2>
- Kaligatla RB, Manisha, Sahoo T (2017) Wave trapping by dual porous barriers near a wall in the presence of bottom undulation. *Journal of Marine Science and Application* 16: 286-297. <http://html.rhhz.net/jmsa/html/20170304.html>
- Kaligatla RB, Tabssum S, Sahoo T (2018) Effect of bottom topography on wave scattering by multiple porous barriers. *Meccanica* 53(4): 887-903. <https://link.springer.com/article/10.1007/s11012-017-0790-2>
- Koley S, Kaligatla RB, Sahoo T (2015) Oblique wave scattering by a vertical flexible porous plate. *Studies in Applied Mathematics* 135(1): 1-34. <https://onlinelibrary.wiley.com/doi/full/10.1111/sapm.12076>
- Krishna KA, Karaseeri AG, Karmakar D (2023) Oblique wave propagation through composite permeable porous structures. *Marine Systems and Ocean Technology* 17(3-4): 164-187. <https://link.springer.com/article/10.1007/s40868-022-00122-1>
- Krishnendu P, Balaji R (2020) Hydrodynamic performance analysis of an integrated wave energy absorption system. *Ocean Engineering* 195: 106499. <https://doi.org/10.1016/j.oceaneng.2019.106499>
- Lee MM, Chwang AT (2000) Scattering and radiation of water waves by permeable barriers. *Physics of Fluids* 12: 54-65. <https://doi.org/10.1063/1.870284>
- Li Y, Liu Y, Teng B (2006) Porous effect parameter of thin permeable plates. *Coastal Engineering Journal* 48(4): 309-336. <https://doi.org/10.1142/S0578563406001441>
- Liu Y, Li Y, Teng B (2007) Wave interaction with a new type perforated breakwater. *Acta Mechanica Sinica* 23(4): 351-358. <https://link.springer.com/article/10.1007/s10409-007-0086-1>
- Manam SR, Sivanesan M (2016) Scattering of water waves by vertical porous barriers: an analytical approach. *Wave Motion* 67: 89-101. <https://doi.org/10.1016/j.wavemoti.2016.07.008>

- Porter D, Staziker DJ (1995) Extensions of the mild-slope equation. *Journal of Fluid Mechanics* 300: 367-382. <https://doi.org/10.1017/S0022112095003727>
- Sahoo T (1998) On the scattering of water waves by porous barriers. *Journal of Applied Mathematics and Mechanics* 78: 364-370. [https://doi.org/10.1002/\(SICI\)1521-4001\(199805\)78:5](https://doi.org/10.1002/(SICI)1521-4001(199805)78:5)
- Sahoo T, Lee MM, Chwang AT (2000) Trapping and generation of waves by vertical porous structures. *Journal of Engineering Mechanics* 126: 1074-1082. [https://doi.org/10.1061/\(ASCE\)0733-9399\(2000\)126:10\(1074\)](https://doi.org/10.1061/(ASCE)0733-9399(2000)126:10(1074))
- Suh KD, Park WS (1995) Wave reflection from perforated wall caisson breakwaters. *Coastal Engineering* 26(3-4): 177-193. [https://doi.org/10.1016/0378-3839\(95\)00027-5](https://doi.org/10.1016/0378-3839(95)00027-5)
- Tabssum S, Kaligatla RB, Sahoo T (2020) Surface gravity wave interaction with a partial porous breakwater in the presence of bottom undulation. *Journal of Engineering Mechanics* 146(9): 04020088. [https://doi.org/10.1061/\(ASCE\)EM.1943-7889.0001818](https://doi.org/10.1061/(ASCE)EM.1943-7889.0001818)
- Venkateswarlu V, Karmakar D (2020) Significance of seabed characteristics on wave transformation in the presence of stratified porous block. *Coastal Engineering Journal*, 62(1): 1-22. <https://doi.org/10.1080/21664250.2019.1676366>
- Williams AN, Wang KH (2003) Flexible porous wave barrier for enhanced wetlands habitat restoration. *Journal of Engineering Mechanics* 129: 1-8. [https://ascelibrary.org/doi/abs/10.1061/\(ASCE\)0733-9399\(2003\)129:1\(1\)](https://ascelibrary.org/doi/abs/10.1061/(ASCE)0733-9399(2003)129:1(1))
- Yip TL, Sahoo T, Chwang AT (2002) Trapping of surface waves by porous and flexible structures. *Wave Motion* 35(1): 41-54. [https://doi.org/10.1016/S0165-2125\(01\)00074-9](https://doi.org/10.1016/S0165-2125(01)00074-9)